Journal of Materials Chemistry B

Accepted Manuscript

ROYAL SOCIETY OF CHEMISTRY

www.rsc.org/materialsB

Journal of Materials Chemistry B

Dynamic Article Links ►

ARTICLE TYPE

Cite this: DOI: 10.1039/c0xx00000x

www.rsc.org/xxxxxx

Topography-dependent Antibacterial, Osteogenic and anti-aging Properties of pure Titanium†

Qiaojie Luo,[a] Ying Huang,[a,b] Guangyu Zha,[a] Yadong Chen,[a] Xuliang Deng,[b] Kai Zhang,[a] Weipu Zhu,[c] Shifang Zhao[a] and Xiaodong Li[a,*]

Received (in XXX, XXX) Xth XXXXXXXXX 20XX, Accepted Xth XXXXXXXXX 20XX
DOI: 10.1039/b000000x

After nearly half a century of development under the guidance of osseointegration theory, the major dilemmas for current implant dentistry are the implant associated infection and insufficient osseointegration. Moreover, biological aging of titanium (Ti) implant also brings great uncertainty to clinical results. In the present study, a novel nano-micro-hierarchical topography pattern is created by sandblasting and dual acid-etchings on Ti surface. The physi-co-chemical properties of the surfaces were characterized by scanning electron microscope, contact angle measurement, X-ray photoelectron spectroscopy and X-ray diffraction. The effects of the hierarchical surfaces on osteoprogenitor cell growth and bacterial activities were separately evaluated. The optimized nano-micro-hierarchical Ti surface exhibits surprisingly topography-dependent antibacterial capacity via inhibiting bacterial adhesion of several species in the early stage and better osteogenesis ability than the microscaled surface. Aging study demonstrates that, compared with the surface with microscale structure, the nano-micro-hierarchical Ti surface has greater anti-aging ability manifested as being more capable to retain hydrophilicity and bioactivity during aging. Furthermore, the present study reveals that the biological aging of the Ti implant is attributed to two decisive factors during aging period: the progressively thickened amorphous TiO_2 layer by autoxidation and the unavoidable accumulation of hydrocarbons on Ti implant surface.

1. Introduction

Dental implant therapy is now widely accepted and revolutionizes dental rehabilitation because of its esthetic, stable and comfortable characters. Since its inception into the modern era of dentistry, a large number of clinical techniques aimed at expanding the clinical indications and improving the success rate have been developed, such as maxillary sinus floor augmentation [1], bone graft [2], guided bone regeneration [3], osteotome technique [4], and zygomatic implant [5]. However, Ti-based implant is still encountered with certain clinical challenges, deficient osseointegration and implant associated infection [6, 7], which is therefore not under the control of the clinician. Modifying the implant surface to achieve higher bioactivity is an alternative approach.

Surface topography has been identified as a crucial property that affects osseointegration [8, 9]. The majority of the commercially available Ti implant surfaces are modified by architecting the surface with microscale features [10], which has been evidenced to enhance osteogenic differentiation and optimize stress distribution [10, 11]. However, biological dilemmas of the microscaled surface are still present: the compromise on osteogenic cell proliferation that challenges the rapid generation of greater amounts of bone [12] and the susceptibility to bacteria due to comparable size to bacteria that maximizes the contact area of bacteria-surface [13, 14]. Once an implant implanted into bone, tissue cell integration and bacterial adhesion compete for the implant's surface. For successful implantation, tissue cell integration wins the bacterial adhesion in such "race for the surface" [15], that is tissue integration occurs before bacterial colonization. Nevertheless, among the currently available implant systems, antibacterial property has rarely been taken into consideration where osseointegration is the main concern. Among the few studies focused on the antibacterial property of Ti implant [7, 16-21], most of them introduced antibacterial agents [7, 16, 18, 20, 21], which could compromise osteogenic property and introduce other potential side effects [18, 21]. Modifying Ti implant surface topography to enhance osseointegration while decrease susceptibility to bacteria would be a challenging but promising approach in current study.

As biological aging of Ti, defined as time-dependent degradation of osseointegration capability of pure Ti [22-24], is inevitable due to the period of distribution and storage before use, it is necessary to uncover the mechanism underlying and develop effective strategies to prevent or alleviate biological aging. Though Ti aging has already been widely studied [22-25], the

mechanism behind Ti aging is still not quite clear and strategy for anti-aging was rarely reported, except for the method developed in SLActive system [26, 27].

In the present study, a series of nano-micro-hierarchical topographies were fabricated on Ti surface through the combination of sandblasting and two acid-etching treatments. It is exciting to find that besides excellent osteoblast response, the optimized nano-micro-hierarchical Ti surface exhibited a surprising topography-dependent inhibitory effect on bacterial adhesion of several species in the early stage. Via comparative investigation of the physi-co-chemical properties and the biological properties before and after aging treatment, we found that Ti surface of nano-micro-hierarchical feature also showed stronger anti-aging ability. Moreover, different from the current point of views on the mechanism of Ti biological aging, we revealed that the thickened amorphous TiO_2 layer by autoxidation and the unavoidable deposition of carbon from the atmosphere on Ti surface are the two decisive factors for Ti biological aging.

2. Results

2.1 Surface topography

The MS0 exhibited large cavities of microscale (20 to 40 μm in diameter) resulting from the large grit sandblasting process, superimposed with micro- and submicroscale compartmental architectures ranging 1-2 μm peak-to-peak distance with sharp ridges (Figure. 1, S1). High magnification SEM images of the MS0 group revealed smoothness at the nanoscale. After the secondary acid-etching, nanoscale structures were produced on the the existing micropits. Simultaneously, the microconfiguration of the original micropits was preserved to a certain extent, with ridges of the micropits slightly rounded and the fluctuations of the microscale structures slightly diminished. The heterogeneous and three-dimensional multiscale structures constructed in the present study were structurally similar with the hierarchical bone tissues in living systems. The prolonged secondary acid-etching time increased the nanopillar structures and weakened the microscale structures. However, compared with the corresponding fresh one, no detectable changes in surface topography were found on the aged samples.

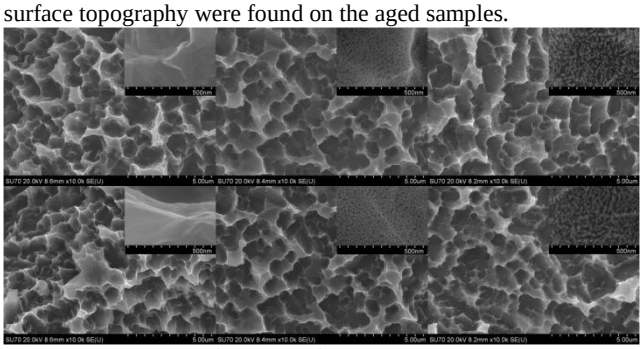

Figure 1. SEM images for MS0 (left panels), MS30 (middle panels) and MS60 (right pannels) of the fresh samples (upper panels) and the corresponding one-month aged smaples (lower panels). No nanostructures were present on the MS0 and One-Aged-MS0, whereas all other groups clearly showed the presence of characteristic nanostructures. No detectable morphological changes were present after one-month storage. Inserted SEM images in the upper right corner show typical high magnification of 100000×, and the scale bar in the insertion was 500 nm.

2.2 Contact angle and SFE

All the groups with nano-micro-hierarchical surface showed superhydrophilicity immediately after preparation (contact angle < 5°. In fact, as soon as the water droplet contacted the surfaces of these samples, it spread out, resulting in a contact angle of 0°, Figure. 2A). The superhydrophilic status of the MS15, MS30, MS45 and MS60 were fairly retained even after aged for one month. The other two groups with nano-micro-hierarchical topography, MS90-Ti and MS120-Ti, the contact angles rose slightly but still below 10° on the one-month-aged samples. But for the microstructured group MS0, the contact angle was about 5° for the freshly prepared samples, and the hydrophilic status immediately started to disappear, and became hydrophobic (over 50°) at the end of one-month aging treatment. All groups became hydrophobic when aged for six months, with contact angles ranging from 110° to 121°.

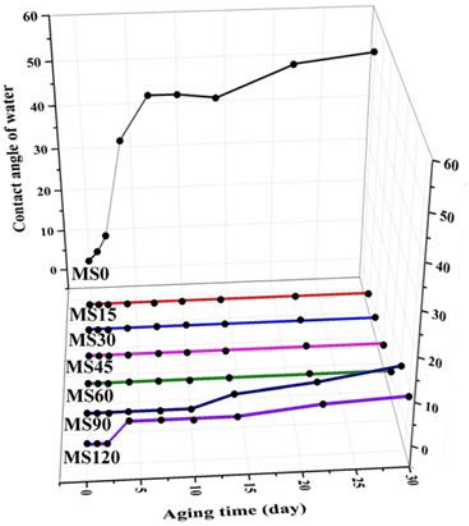

A

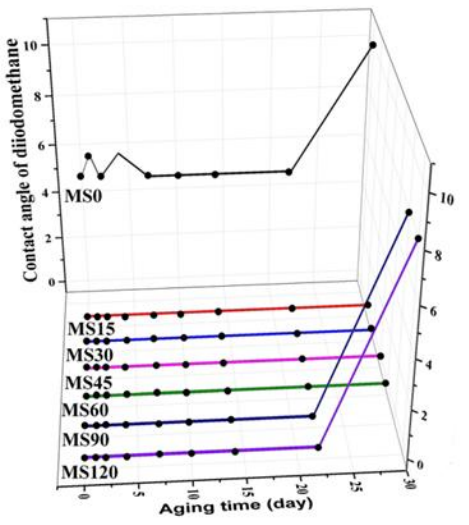

B

Figure 2. Contact angle measurement with deionized water (A) and

diiodomethane (B) as probing liquids. A time-relating and surface-depending pattern can be observed. Surfaces with nano-micro-hierarchical topography showed superhydrophilic and superoleophylic and four of them kept superamphiphilic during the testing time.

When diiodomethane was used as the probing liquid, the same changing trend as that in the water contact angle was found (Figure. 2B). The contact angles for all the groups with nano-micro-hierarchical surface were kept near 0 ° for more than twenty days, and only that for the MS120 rised to 8 °while others still kept 0 ° after one entire month of aging treatment. However, the contact angle for the microstructured group was about 6 ° at the beginning and rised over 10 °at the end of one-month aging.

SFE was calculated based on the contact angles of deionized water and diiodomethane (Table 2). Samples showed amphiphilic were of high SFE and the increase of contact angle indicated the decrease of the SFE. Though the difference within the groups of nano-micro-hierarchical surfaces cannot be reflected because of the limitation of the method employed, groups with only microstructure feature had significantly lower SFE during the entire experiment period. Moreover, SFE of the MS0 descended most quickly, led to the difference of SFE between MS0 and the other groups increase during the first one-month aging. These foundings indicated that the nano-micro-hierarchical surfaces had stronger retention capacity of hydrophilicity and SFE than the microstructured surface during aging.

Table 1. SFE parameters for the two probing liquids (mJ/m2)

Liquids	γ^{LW}	γ^{+}	γ^{-}	γ^{AB}	γ^{TOT}
Deionized water	21.8	25.5	25.5	51	72.8
Diiodomethane	50.8	0	0	0	50.8

Table 2. SFE calculation (mJ/m^2)

Aging time (day)	1	2	3	5	8	11	15	23	30
MS0	81.15	80.91	80.33	72.44	67.53	67.53	68.03	64.47	63.26
MS15	a	a	a	a	a	a	a	a	a
MS30	a	a	a	a	a	a	a	a	a
MS45	a	a	a	a	a	a	a	a	a
MS60	a	a	a	a	a	a	a	a	a
MS90	a	a	a	a	a	a	a	a	80.64
MS120	a	a	a	a	a	a	a	a	80.64

[a] SFE cannot be calculated when either of the contact angle was 0 °.

2.3 XRD patterns

The XRD spectra in Figure. 3 disclosed that peaks of metallic Ti and TiH_2 were visible in all the surfaces. No characteristic peaks related to crystalline TiO_2, either anatase or rutile, were detected in any sample. Moreover, all the samples after the storage under dry ambient conditions for one month and six months exhibited identical peaks with that detected from the freshly prepared samples.

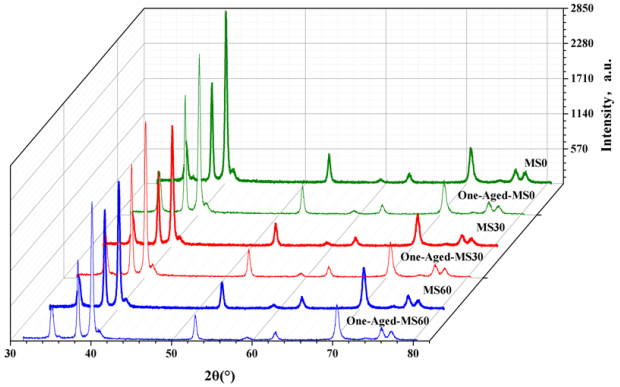

Figure 3. XRD patterns. XRD analysis revealed that there were no detectable changes in the chemical phases between samples with different topographies and between moreover, sample before and after one-month aging.

2.4 XPS analysis

The XPS spectra revealed that Ti, C, N and O were present on all surfaces. The Ti2p high-resolution spectra were all deconvoluted into four sub-peaks (Figure. 4). The peak components of Ti2p can be attributed to Ti in the oxidation states IV (TiO_2), III (Ti_2O_3), II (TiO) and 0 (Ti ^{metallic}). The dominant $Ti2p_{3/2}$ peak at binding energy around 459 eV can be assigned to TiO_2. A small peak at ~454 eV is typical for metallic Ti. A shoulder at ~ 457 eV was assigned to Ti_2O_3, while the shoulder at ~455 eV was assigned to TiO. The lower valence states Ti (III) and Ti (II) might be due to defined suboxide phases. The Ti ^{metallic} peak containing in the Ti 2p peak would be explained by the contribution from the metal below the surface oxide. As the secondary acid-etching time was prolonged, the relative areas of Ti ^{metallic}, TiO and Ti_2O_3 decreased, while that of the TiO_2 increased (Figure. 4 C). After aging treatment, the relative areas of Ti ^{metallic}, TiO and Ti_2O_3 decreased while that of the TiO_2 increased in all groups. The trends of the relative content of each component among the aged-groups of the same aging time were the same as that in the fresh groups.

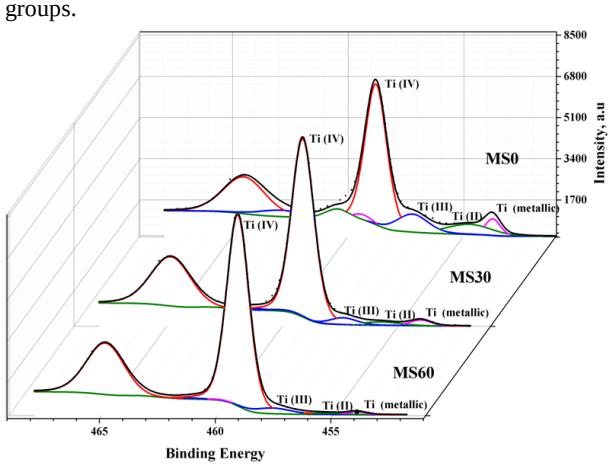

A

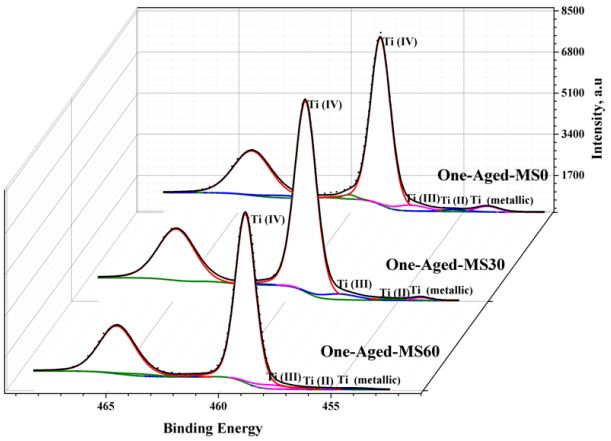

Figure 4. XPS analysis. Results of the deconvolution of Ti 2p of the freshly prepared (A), one-month-aged (B) and six-month-aged samples (C) and relative content of surface elemental composition (D). * $p < 0.05$, compared with the same chemical species of the corresponding microscaled group with the same aging time.

Deconvolution of high resolution spectra of the C1s revealed that the C1s peak was dominated by a peak at 284.6 eV, which can be attributed to hydrocarbons (C-C and C-H bonded carbon). Two carbon subpeaks at ~286.1 and ~288.4 eV were also observed, which were corresponding to C-O and C=O species, respectively [25] . No differences in the relative fraction of each component among the groups were found (p=0.63, Chi-Square Tests). The consistency of composition and concentration indicated that its source probably was the adsorbed carbon compounds from the ambient air. Relative concentration of C in C, N, O and Ti was similar among the groups (from 17.38% to 18.50%). After one-month aging treatment, the components of C remained the same, while the relative concentration of C was increased in all samples (within the range of 30.72% to 32.13%) without significant difference among the one-month aged groups. After six months of aging treatment, no significant difference in carbon concentrations was observed when compared with the one-month-aged groups ($p>0.05$).

2.5 Cell differentiation

ALP is a marker of early osteogenic differentiation. In all groups, ALP activity increased with incubation time (Figure. 5A). The MS30 group showed the highest ALP activity at all the time points with statistical significance ($p<0.05$). However, ALP activity of the MS60 was lower than that of the MS0, although the difference was not statistically significant. The ALP activity of all the aged groups did not reach the level achieved by the freshly prepared groups. However, the decrease rate was different during aging, with the MS0 decreasing most quickly. Among the one-month-aged samples and the six-month-aged samples, the One-Aged-MS30 and the Six-Aged-MS30 had the highest ALP activity ($p<0.05$), respectively. Unlike the fresh samples, where the ALP activity of MS60 group was lower than that of the MS0 ($p>0.05$), the ALP activity of One-Aged-MS60 and the Six-Aged-MS60 were higher than the One-Aged-MS0 and the Six-Aged-MS0, respectively ($p>0.05$).

Consistent with the increased ALP activity on the nano-micro-hierarchical surface, OC production of the MS30-Ti group were the most, followed by the MS0 and MS60 group with statistical significance between any two of them ($p<0.05$). Less OC production on the aged groups than on the newly prepared groups was observed on all the groups (Figure. 5B). For the six-month-aged samples, OC production was further decreased. Similarly, MS0 decreased most sharply (31.49% for the one-month-aged group and 50.59% for the six-month-aged group). The OC productions of the One-Aged-MS0 was lower than that of the One-Aged-MS60 ($p>0.05$). When aged for six months, OC production level of the Six-Aged-MS0 was lower than the Six-Aged-MS60 with statistical difference ($p<0.05$).

The area of mineralized nodules detected by alizarin red S staining was largest on MS30 and smallest on MS60 among the fresh samples. After one month aging treatment, the order varied, with the content in descending order as follows: One-Aged-MS30, One-Aged-MS60 and One-Aged-MS0 (Figure. 5 C, D).

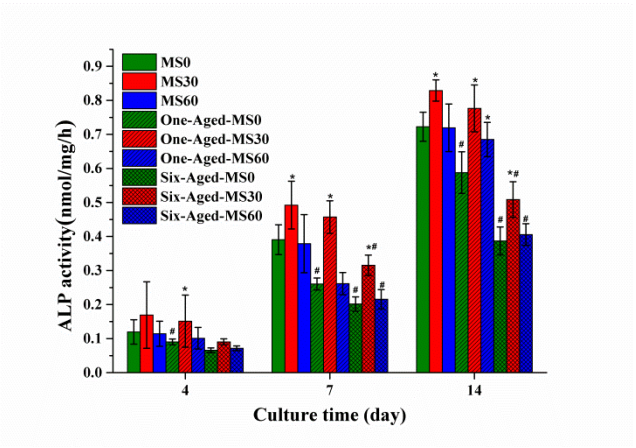

A

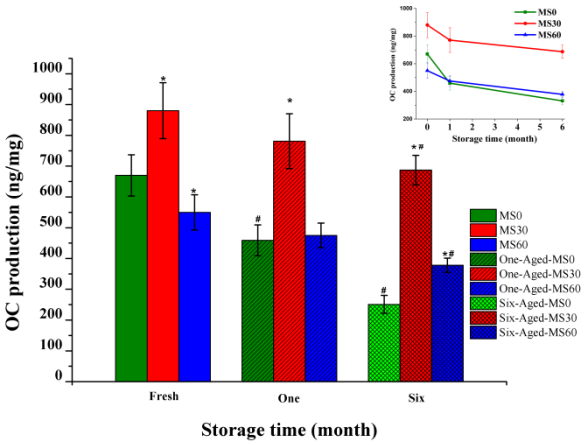

B

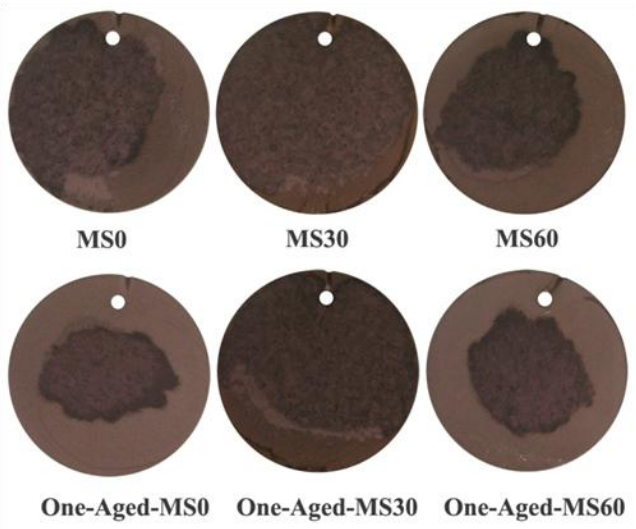

C

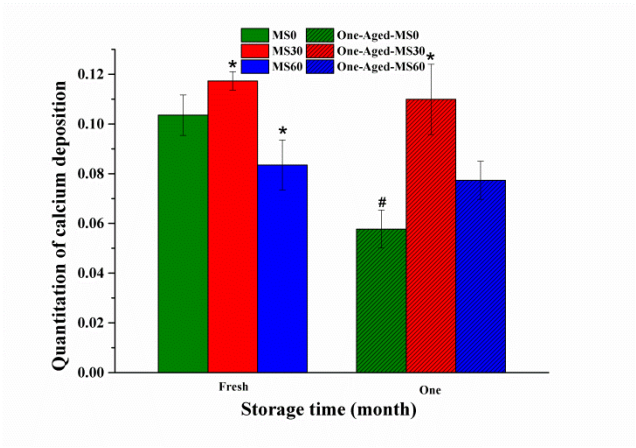

D

Figure 5. Cell differentiation determined by ALP activity (A), OC production (B), alizarin red staining images (C) and total calcium deposition, measured using a colorimetry-based method (D). Within each group, fresh or aged, MS30 expressed the highest differentiation markers and had the most calcium deposition. Compared with the corresponding freshly prepared surfaces, the aging treatment showed differentiated impact on the bioactivity of different surfaces. * $p < 0.05$, compared with the corresponding microscaled group with the same aging time; # $p < 0.05$, compared with the corresponding fresh group of the same topography.

2.6 Antibacterial ability

SEM examination showed that much less bacteria were on nano-micro-hierarchical topography (both MS30 group and MS60 group) than that on micro-structured topography (MS0 group) for both Gram-negative bacteria (E. coli and P. vulgaris) and Gram-positive bacterium (S. aureus) (Figure. 6A~C). Furthermore, on micro-structured topography, E. coli and P. gingivalis bacterial cells displayed intact rod-shape (E. coli and P. vulgaris) or grape-shape (S. aureus) and more binary fission of bacterial cells were observed.

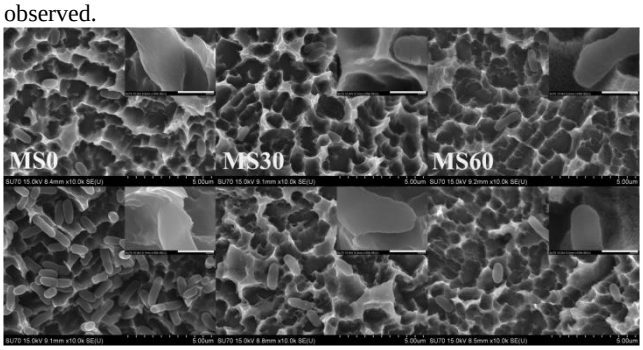

A

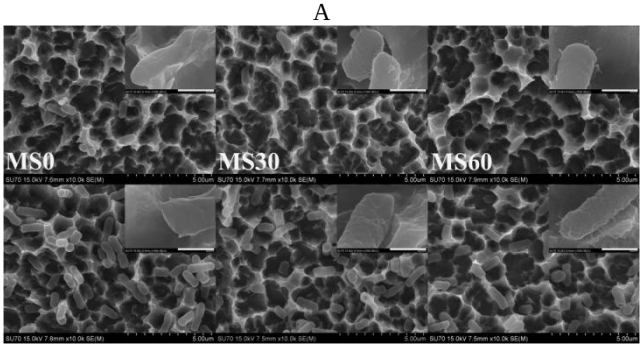

B

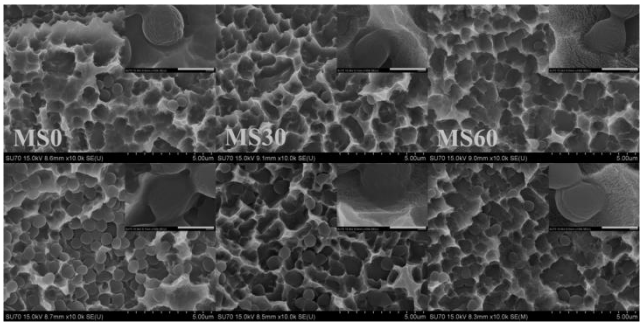

C

Figure 6. Morphology observation by SEM of E. coli (A), P. vulgaris (B) and S. aureus (C) retention on different surfaces after cultivation for 0.5 h (top) and 6 h (bottom). Inserted SEM images in the lower right corner show typical cell morphologies with magnification of 100000×. The scale bar in the insertion was 500 nm.

The antibacterial effects of the nano-micro-hierarchical topography were intuitively investigated by dyeing experiment (Figure. 7A~C). As time progressed, the number of bacteria on all the surfaces increased. At each time point, bacteria preferentially adhered to the MS0 group. Bacteria on the MS30 group and MS60 group were much less than that on the MS0 group.

CV staining test was used to further quantitatively evaluate the antibacterial activity (Figure. 8A~C). CV assay showed that not only the fleshly prepared nano-micro-hierarchical groups restrained the adhesion of all the tested strains, but also did the aged ones. More bacteria adhered on the aged samples when compared to the corresponding fresh one. At each time point, most bacteria were on the MS0 and the One-Aged-MS0 group among the freshly prepared groups and the one-month-aged groups, respective ($p<0.05$), especially at longer culture time (12 h in the present study).

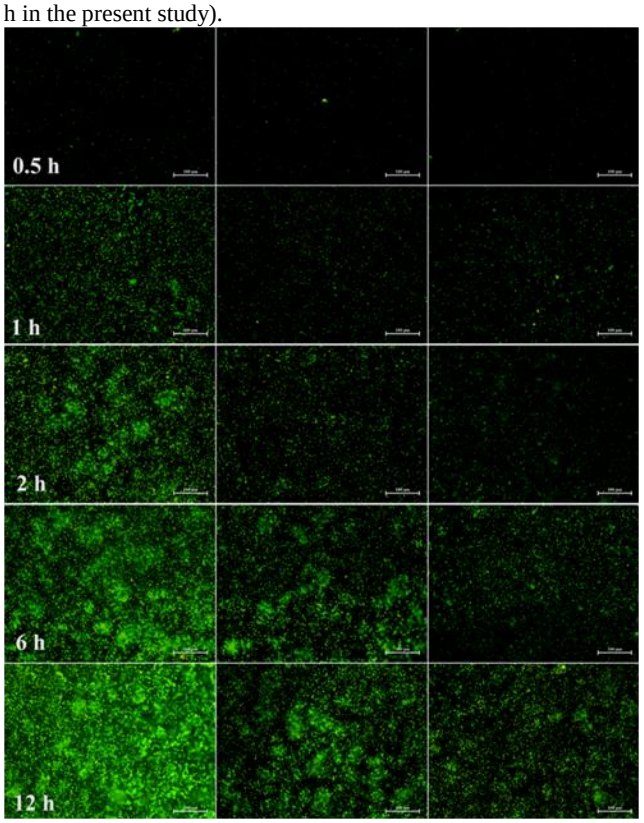

A

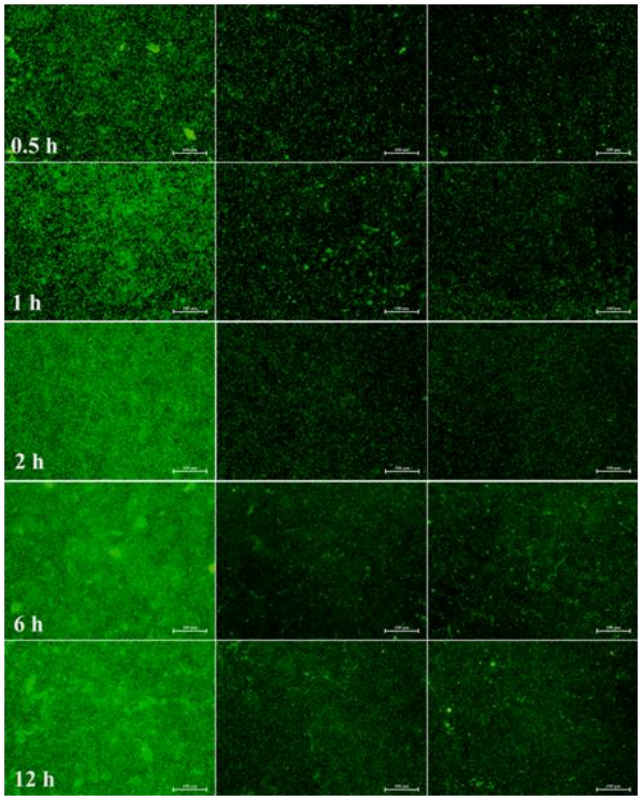

B

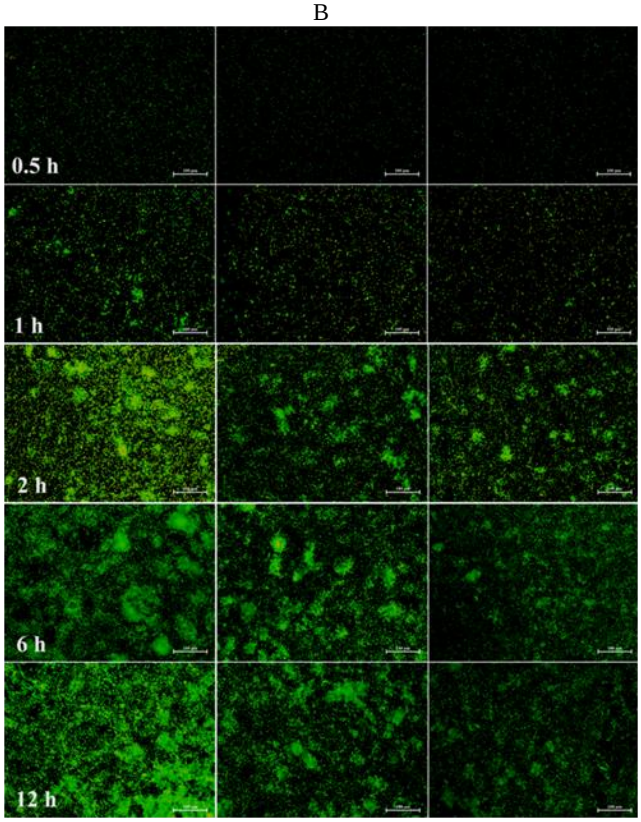

C

Figure 7. Bacteria stained with Live/Dead Bacterial Viability Kits. More bacterial cells retained on the MS0 group (the left panels) than that on the MS 30 (the middle panels) and the MS 60 (the right panels) at any tested time point for all three tested strains: E.coli (A), P.vulgaris (B) and S.aureus (C). Scale bars in the fluorescent images were 100 μm.

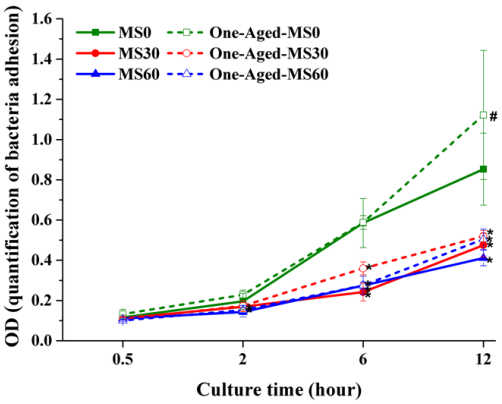

A

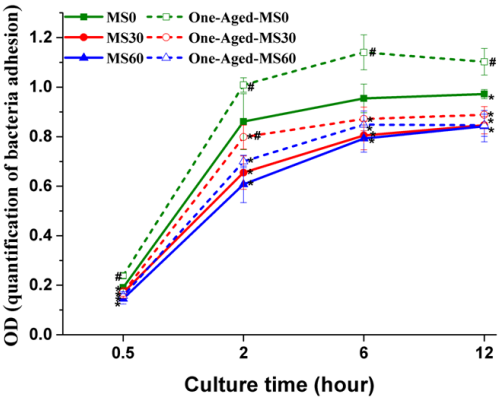

B

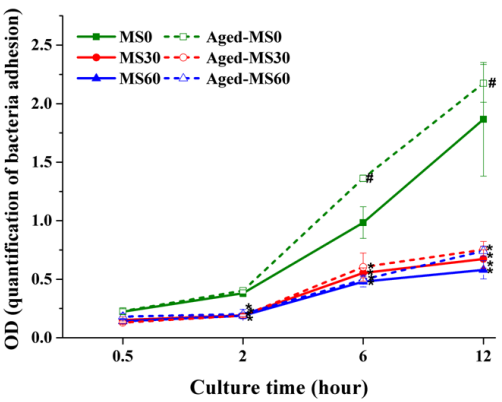

C

Figure 8. Quantitative determination of bacterial retention on different surface topographies with different storage times by crystal violet staining: (A) E. coli, (B) P. vulgaris and (C) S. aureus. * $p < 0.05$, compared with the corresponding microscaled group with the same aging time; # $p < 0.05$, compared with the corresponding fresh group of the same topography.

3. Discussion

Generally, several aspects of the Ti surface were suspected to influence tissue response and bacterial colonisation, including chemical composition, cystalline phase, surface topography, SFE and surface hydrophilicity [21, 26-28]. Characterization of the freshly prepared samples showed that, as the second acid-etching time increased, the nanoscale structure strengthened, while the microscale structure weakened (Figure. S1). Moreover, the thickness of the oxide layer of amorphous TiO_2 increased, which was manifested as the gradually weakened signal of the $Ti^{Metallic}$ and the decrease in the area proportion of the subpeaks for Ti (II) and Ti (III) (Figure. 4A, B) based on the limiting probing depth of XPS detection [29] and the three different layer model for the oxide film [30]. Surface wettability is governed by surface chemistry and microstrucure [31, 32]. Although all the samples showed good hydrophilicity immediately after preparation, the nano-micro-hierarchical groups showed higher hydrophilic than the group of pure microscale structure, manifested as the fact that once the disc of nano-micro-hierarchical surface contacted with a water droplet, a film can propagate along the surface rapidly. As the chemical compositions of all the samples were almost the same, such phenomenon could be explained by the theory of the three-dimensional (3-D) capillary effect of a rough surface, which describes water will enter and fill the interstices among the hierarchical structures [33]. Combining with the consistent chemical composition of all the groups, such phenomenon suggested that the geometrical topography structure of the surface led to the difference in the wettability.

After one month of aging treatment, no detectable changes in surface topography, composition and crystalline phases were found (Figure. 1, 2), except that the oxide layer of amorphous TiO_2 of all the samples was markedly thickened (Figure. 4A, B). Moreover, carbon compounds accumulated on all samples, as was reported previously [22]. However, the hydrophilicity and lipophilicity of all the samples were differentially maintained (Figure. 2). The continuously increased contact angle on the microstructured surface and the well-remained superhydrophilicity on the nano-micro-hierarchical surfaces revealed that the nano-micro-hierarchical surfaces possessed stronger hydrophilic retention ability than the microstructured surface during aging. Within the nano-micro-hierarchical groups, the inconsistent change in hydrophilicity could mainly stem from the difference in the size, distribution and spacing of the microscale structure and nanoscale structure. Clearly, nano-micro-hierarchical Ti surfaces possessed higher hydrophilicity and stronger retention ability of hydrophilicity. Moreover, optimized assembly of microstructures of each scale could maximize these properties. Excessive loss of microscale structure with the increasing of nanoscale structure weakened the retention ability of hydrophilicity of MS90 and MS120 groups.

After six-month aging treatment, the thickness of the oxide layer of amorphous TiO_2 of all groups got further increased, and the contact angle of hierarchical surfaces from MS15 group to MS60 group showed remarkable increase, rising from 0 ° to about 100 °; close to that on the MS90 and MS120 group of the same aging period. However, the amount of carbon compounds accumulated on each group was only slightly increased when compared with the corresponding one-month-aged samples. Taking the consistent resultant surface composition, the same crystalline phase, the same aging time span into consideration, the degenerative hydrophilicity of all samples should be attributed to the thickened oxide layer of amorphous TiO_2 and the

accumulated carbon compounds.

Inhibiting the initial bacterial adhesion would be more effective to reduce the risk of bacteria-associated infection, because bacteria encapsulated within biofilm are less susceptible to hazardous substances [34]. In the present study, the adhesion on the nano-micro-hierarchical surfaces of all three species, involving gram-negative and gram-positive bacteria, was markedly inhibited during the first 6 hours (Figure. 6-8). As the first several hours after implantation is regarded as the most vulnerable period to infection [35], the nano-micro-hierarchical surface would be effective in preventing perioperative infection. Bacterial adhesion to abiotic surfaces is strongly affected by the physic-co-chemical properties of both the substrate surface and the bacterial cell wall. Antibacterial ability of the nano-micro-hierarchical surface might be attributed to the following three aspects. Firstly, the presence of the nanoscale structures in the nano-micro-hierarchical surface could lead to a reduction in the available contact area for the bacteria. At the initial stage of bacteria-substrate interaction, extracellular cell matrix is not necessary and appendages like flagella and pili might play an important role [36]. The bacterial cell membrane was rigidity, which would lead to more energy cost in terms of elastic energy upon distorting [37]. Moreover, the size of a bacterium ranged from hundreds of nanometers to a few microns [38], dramatically larger than the nanoscale structure of nano-micro-hierarchical surfaces. From this perspective, the strengthening in nanoscale structure combing with the weakening in microscale structure of the nano-micro-hierarchical surface reduced the available contact area and would be an unfavourable factor for bacterial adhesion. Secondly, the superhydrophilicity of the nano-micro-hierarchical surface also contributed to the antibacterial ability. When two surfaces come together, absorbed water must be displaced [39]. The displacement of water on the highly hydrated nano-micro-hierarchical surface could be energetically unfavourable and difficult to overcome by the counteracting attractive interactions, which was also observed in other studies [40]. Thirdly, the high surface energy of the nano-micro-hierarchical surface might contribute to the bacterial deformation and growth inhibition.

It has been reported that superhydrophobic surfaces with low surface energy are not susceptible to colonization because of the minimum intermolecular forces allowing the adhered organism to be easily detached from the surface [41]. Surface modified with highly hydrophilic polymers also exhibited a low degree of bacterial adhesion [42], through generating hydration layers to reduce direct interactions between bacteria and the surfaces. Ti surface was modified with 1H, 1H, 2H, 2H-perfluorooctyl-triethoxysilane to form superhydrophobic surface with the aim to reduce bacterial adhesion [43]. However, hydrophobic implant surface has been proved to be unfavourable for the early stage of osseointegration [44]. Hydrophilic polymer immobilization for the antibacterial purpose also showed decrease in eukaryotic cell adhesion [45]. The topography-dependent antibacterial property would provide an alternative way that would not compromise the osteogenesis of the implant.

Osteoblastic cells showed sensitivity to the topographical modifications and the aging treatment (Figure. 5). The highest level of phenotypic expression was observed on the MS30, One-Aged-MS30, and Six-Aged-MS30 among the fresh groups and the aged groups respectively, suggesting that this surface was superior in eliciting a cell response that favours osteogenesis. The different mechanism involved in interactions of cell-substrate from that of the bacteria-substrate should account for the apparently different response. Cells interact with substrates through integrins [46]. Surface topography and surface hydrophilicity could influence the adsorption and conformation of the ligands for integrins and thus influence cell adhesion [47]. The appearance of nanoscale structure increased the special surface area, which could provide more sites for protein adsorption. At the same time, hydrophilic Ti surfaces were supposed to lead to a gentle interactions with the water shell around delicate biomolecules [48]. As a result, the superhydrophilic nano-micro-hierarchical surface could adsorb more proteins in favour of osteogenesis and influence their conformation, and thus regulate the recruitment of integrins and then cell adhesion. The superhydrophilicity and the retention of the high hydrophilicity during aging treatment could contribute to the higher bioactivity of the aged nano-micro-hierarchical groups than the aged miroscaled groups. During bone healing, new bone formed on the areas where micro-cracks were removed by osteoclasts [49]. Resorption lacunae left by osteoclasts have a distinct hierarchical structural complexity, consisting microscale pits with submicro-scale roughness and nanoscale features [50]. The heterogeneous and three-dimensional features of the nano-micro-hierarchical structures were structurally similar with the hierarchical structure created by osteoclasts and might provide more environment cues to osteogenesis. However, the weakening of the microscale structure led to a smaller surface roughness (Figure. S2), which could result in the poorer performance of the MS60, as surface roughness was regarded as a contributing factor to bone cell differentiation [51].

After aging treatment, both the antibacterial effect and the osteoblast differentiation of all groups were compromised (Figure. 5, 8). However, either the antibacterial ability or the pro-osteogenic capacity was better kept on the groups with nano-micro-hierarchical surface topography than the microscaled group, which was evidenced by the largest degradation rate of MS0 group during the same aging period (Insertion in Figure 5B). This should be attributed to the better retention ability of hydrophilicity and higher SFE of the hierarchical Ti surfaces. These results indicated that the nano-micro-hierarchical surfaces had an even greater anti-biological-aging capacity compared to the microstructured surface.

Previous studies found that the degradation of biological properties of the aged Ti implant was accompanied with the progressive accumulation of hydrocarbons and time-related disappearance of hydrophilic property of Ti surface [22, 24]. Moreover, after ultraviolet (UV) treatment, the osteogenic activities of aged Ti implant could be temporarily recovered, with the carbon content being reduced and surface wettability improved [52]. Thus, current researchers attribute biological aging of Ti implant to the accumulation of hydrocarbons and the disappearance of hydrophilicity. However, the reasons for the quick attenuation of the recovered bioactivity and hydrophilicity after UV functionalization were still kept unknown. Therefore, there must be some factors of the nature of Ti material itself involved.

According to the results present in this study, the time-dependent degradation of Ti bioactivity can be attributed to the thickened amorphous TiO_2 layer by autoxidation and the deposition of carbon from the atmosphere during aging, which also determined the degradation in hydrophilicity of the resultant Ti surfaces. Once fresh Ti implants are exposed to air, the process of oxidation and the contamination of hydrocarbons are inevitable. The naturally formed oxide layer of pure Ti was reported to be unstable [53] and bioinert [54], and UV treatment can be employed to surmount the resultant degradation[52] . It is well accepted that TiO_2 crystalline film (both anatase and rutile) can create surface oxygen vacancies at bridging sites under UV irradiation, resulting in the conversion of relevant Ti^{4+} sites to Ti^{3+} sites [55], which induce a series of photocatalytic reactions to degrade the contaminated hydrocarbons [56] and at the same time, improve surface hydrophilicity [57, 58]. Herein, according to the results present in this study, the photo-induced biological effects on pure Ti surface with amorphous TiO_2 might be obtained through similar mechanism. Under UV irradiation, the hydrocarbons accumulated on the aged Ti would be degraded by photocatalysis accompanied with the improvement of surface hydrophilicity induced by the conversion of relevant Ti^{4+} sites to Ti^{3+} sites of amorphous TiO_2 film by autoxidation [57, 59]. The amorphous TiO_2 layer did not change during UV treatment, thus leading to the quick attenuation of the recovered bioactivity and hydrophilicity after UV functionalization when the electron-hole pairs created during UV irradiation recombined. The experiment phenomena that the quick attenuation in the recovered bioactivity and hydrophilicity was out of sync with the reaccumulation of hydrocarbons, can be perfectly explained by such reasoning, which can't be explained by the existing aging theory. Therefore, anti-aging strategy of pure Ti implant can be developed based on the principle of retarding the oxidation process and reducing the accumulation of hydrocarbons. Actually, the method used to alleviate biological aging of Ti implant, rinsing the acid-etched Ti under nitrogen protection and storing it under the liquid condition [44, 60], completely meets the principle.

4. Experimental Section

4.1 Sample preparation

Commercially pury Ti discs (30 mm in diameter, 1 mm in thickness, Zhejiang Guangci Biomedical Instrument Company, CH) or plates (8 mm × 8 mm × 1 mm) were submitted to mechanical and chemical treatments. The discs were ground with SiC paper of 320 grid, followed by sandblasted with carborundum with the particle size of 250 μm to 400 μm. The sandblasted Ti discs were then successively ultrasonic cleaned with acetone, ethanol and deionized water, and dried with nitrogen blow. The chemical etching was done in two stages. The cleaned discs were firstly acid-etched with a boiling mixed acid containng 6 volume of 98% H_2SO_4, 1 volume of 36% HCl and 5 volume of deioned water for 1 min. After thoroughly rinsed with deionized water and dried with nitrogen blow, samples were bathed in a mixture of 98% H_2SO_4 and 30% H_2O_2 with equal volume proportion at room temperature for different times. Groups were named according to the time of the secondary acid-etching, for example, the MS0 group was not treated with the second acid etching while the MS60 group was treated for 60 min.

Aging samples were first prepared with the identical procedure as the fresh samples, and then packed dry under ambient conditions for 30 days, named One-Aged-MS0, One-Aged-MS30, One-Aged-MS60, *etc*. Samples aged for 6 months were named Six-Aged-MS0, Six-Aged-MS30, Six-Aged-MS60.

4.2 Physi-co-chemical characterization

4.2.1 Surface topographic analyse

Analysis of surface topography was carried out by a field emission scanning electronic microscope (FESEM, SU-70, Hitachi, JP). Scanning electron micrographs were taken at different magnification in the secondary electron mode with a beam voltage of 20 keV after sputter coating with platinum.

4.2.2 Surface wettability measurement and surface free energy calculation

Surface wettability was assessed by measuring the contact angle using an automated contact angle measuring device (GBX Instruments, Valence, FR) at ambient temperature employing the pendant-drop measuring method. The two probe liquids used were the polar liquid, double-distilled water and the non-polar liquid, diiodomethane. At least five measurements were conducted on each surface to obtain the average values. Surface free energy (SFE) was calculated according to the Owens-Wendt method [61]. Parameters used for SFE calculation were provided in Table 1. The total SFE was expressed as a sum of dispersion (γ^d) and polar intermolecular (γ^p) force components.

$$\gamma = \gamma^p + \gamma^d \quad (1)$$

The SFE of each surface was directly obtained from the following equation.

$$(1+\cos\theta)\gamma_L = 2\left(\sqrt{\gamma_L^p \gamma_S^p} + \sqrt{\gamma_L^d \gamma_S^d}\right) \quad (2).$$

Where θ is the contact angle, the subscript L is abbreviated for liquid while S for substrate.

4.2.3 Chemical phase detection with X-ray diffraction

X-ray diffraction (XRD) data were acquired using an X-ray diffractometer (X'Pert PRO, PANalytical, NL) with Cu Kα1(λ= 1.540598 Å)/Kα2 (λ= 1.544426 Å) radiation with the ratio of 0.5, operating at 40 kV and 25 mA with a scan step size of 0.0167113 °.

4.2.4 Chemical composition measurements with X-ray photoelectron spectroscopy

The chemical composition of the surfaces was evaluated by X-ray photoelectron spectroscopy (XPS, Kratos AXIS-Ultra DLD, Shimadzu, JP) under high vacuum conditions. Relative concentrations of the detected elements were calculated by taking the percentages of their peak-to-peak heights in differentiated survey spectra, and after correction by atomic sensitivity factors.

4.3 Bioactivity characterization

4.3.1 Cell culture

MC3T3-E1 cells (Cellbank of the Chinese Academy of Science, CN) were cultured in α-minimum essential medium (Invitrogen Co., US) in the presence of 10% fetal bovine serum (Invitrogen Co.) at 37℃ in a humidified atmosphere of 5% CO_2 with the growth medium refreshed every 3 days. Cells were detached at 90% confluence using 0.25% trypsin-1mM EDTA-4Na and subcultured onto either the freshly prepared or aged Ti disks at a density of 1.0×10^5 cells/disc. The culture medium was replaced with mineralization medium 24 h after seeding and renewed

every 3 days. Mineralization medium was prepared by supplumenting ascorbic acid (Sigma, US) and β-glycerophosphate (Sigma, US) into the growth medium to achieve the final concentration of 50 μg/ml and 10 mM, respectively. The day when the mineralization medium was first added was recorded as day 0.

4.3.2 Alkaline phosphatase activity assay

Alkaline phosphatase (ALP) activity was measured at day 4, day 7 and day 14 using a commercial phosphatase substrate kit (Wako Pure Chemical Industries Ltd., JP) following the specification, and normalized by total protein, which was determined with a bicinchoninic acid (BCA) protein assay (Beyotime Institute of Biotechnology, CN) as described previously [62].

4.3.3 Osteocalcin production

The levels of osteocalcin (OC) in the conditioned media were measured using a commercially available enzyme immunoassay (Mouse Osteocalcin EIA kit, Biomedical Technologies Inc., USA). OC production level was normalized by the total protein and expressed as nanograms of OC per microgram of total protein.as described previously [62, 63].

4.3.4 Calcium deposition

The mineralization capability of osteoblasts on different Ti surfaces was examined by alizarin red S staining. After 28 days of differentiation culture, the specimens were washed twice with 0.01M PBS and fix with pure alcohol for 10 min at room temperature. After that, samples were washed with PBS and stained for 30 min with 0.1% alizarin red S buffered by Tris-HCl solution (pH 8.3). Then, the specimens were rinsed thoroughly with distilled water and dried in air. The stained specimens were photographed. For the quantitative determination of calcium deposition, the stained samples were dissolved in equal volume of 10% hexadecylpyridinium chloride. After shaking for 15 min at room temperature, 100 μl solution of each well was transferred to 96 wells, and color intensity was measured with a microplate reader Spectra Max M5 (wavelength 570 nm, Molecular Devices, LLC, USA).

4.4 Antibactierial assay

4.4.1 Bacterial culture

Antimicrobial activity was determinced by measuring the adhesion and propagation of Staphlococcus aureus (S. aureus), Escherichia coli (E. coli), and Proteus vulgaris (P. vulgaris) on Ti plates. All the strains were kindly supplied by the Department of Medical Microbiology and Parasitology, College of Medicine, Zhejiang University, China.

A loop of glycerol stock of E. coli strain, P. vulgaris strain or S. aureus was streaked onto a Luria-Bertani (LB) medium agar plate and incubated overnight at 37 ℃. Then, a single colony was picked and grown in LB liquid medium at 37 ℃ with shaking (220 rpm) until they reached exponential phase for bacterial growth.

Ti plates prepared as above were plated in 48-well plate. Bacterial cells were seeded at a density of 10^8 CFU per well (McFarland scale score 1), and cultured in humidified environment (37 ℃) for 0.5, 2, 6, and 12 hours.

4.4.2 Morphology characterization

At prescribed time, 0.5 h and 6 h, the media was aspirated, and the Ti plates were washed twice with PBS. The bacteria were fixed with 2.5 % glutaraldehyde at 4 ℃ for 30 min and then dehydrated with graded ethanol solution (35%, 50%, 75%, 90%, 95%, 100% twice) each for 10 minutes at room temperature. Finally, samples were dried by hexamethyl disilazane (HMDS) for 30 min and observed with a field emission scanning electron microscope (FESEM, SU-70, Hitachi, JPN) at voltages 15 kV after the surfaces sputter coated with platinum.

4.4.3 Fluorescent staining

The viability of bacteria on Ti discs with different surface topographies was investigated by staining with LIVE/DEAD Baclight bacteria viability kits (L7012, Molecular Probes, Life Technologies, USA). After exposure to the bacteria suspension of 10^8 cells/ml in at 37 ℃ for 0.5 h, 2 h, 6 h and 12 h, Ti discs were washed with PBS and stained with the combination dye (propidium iodide and SYTO 9) and subsequently recorded with a Olympus fluorescence microscope equipped with a 100W Hg lamp. The viable cells appeared green under the light microscope while non-viable or membrane compromised cells appeared red.

4.4.4 Crystal violet staining

To quantitatively assess the bacteria settled on the samples, the optical density of dissolved crystal violet (CV) from adhered and stained bacterial cells was measured [64]. After the media was aspirated and washed twice with PBS at the end of the culture period, samples were stained with 1% CV for 15 min at room temperature. Excess dye was removed by washing with deionized water. After air dry, 200 μl of 95% ethanol solution were added into each well to dissolve the combined CV. Then the ethanol solution was transferred to 96-well plate and quantified with a microplate reader Spectra Max M5 (wavelength 570 nm, Molecular Devices, LLC, USA). The OD values of CV reported for each group are from 5 samples.

4.5 Statistical analysis

Data were analyzed by ANOVA using the SPSS 16.0 software (SPSS, Inc., US). $p<0.05$ was considered significant. All experiments were repeated three times to avoid the randomness of the observation. Data shown was from one representative experiment.

5. Conclusion

In the present study, topography-dependant antibacterial adhesion ability and osteogenic capacity of Ti implant were simultaneously achieved through fabricating a novel nano-micro-hierarchical topography pattern on Ti surface. Moreover, the nano-micro-hierarchical Ti surface showed outstanding features in alleviating aging. This type of novel nano-micro-hierarchical implants was of promising clinical application. Furthermore, for the first time, we revealed that the thickened amorphous TiO_2 layer by autoxidation and the accumulation of hydrocarbons on Ti surface from ambient air were the two decisive factors for degradation of hydrophilicity and biological aging of the Ti implant. The mechanism underlying the biological aging discovered in the present study would provide theoretical guidance for anti-aging research on Ti implants. This study opened a door to develop a new generation of antibacterial, osteogenic and anti-aging Ti implants.

Acknowledgement

This study was financially supported by the National Natural Science Foundation of China (51173163), the National Science-technology Support Plan project of China (2012BAI07B01), the National Basic Research Program of China (2012CB933900) and the fundamental Research Funds for the Central Universities (2012QNA7043). Qiaojie Luo and Ying Huang contributed equally to this work.

Notes and references

[a] *The Affiliated Stomatology Hospital, College of Medicine, Zhejiang University, Hangzhou, P. R. China. Fax: +8657187217433; Tel: +8657188208378; E-mail address: cisarli@zju.edu.cn*
[b] *Department of Geriatric Dentistry, Peking University School and Hospital of Stomatology, Beijing, P.R. China*
[c] *MOE Key Laboratory of Macromolecular Synthesis and Functionalization, Department of Polymer Science and Engineering, Zhejiang University, Hangzhou, P.R. China*
† Electronic Supplementary Information (ESI) available: See DOI: 10.1039/b000000x/

1. I. Woo and B. T. Le, *Implant dentistry*, 2004, **13**, 28-32.
2. P. Astrand, P. G. Nord and P. I. Branemark, *International journal of oral and maxillofacial surgery*, 1996, **25**, 25-29.
3. J. P. Fiorellini, D. M. Kim, Y. Nakajima and H. P. Weber, *The International journal of periodontics & restorative dentistry*, 2007, **27**, 287-294.
4. R. B. Summers, *Compendium*, 1994, **15**, 152, 154-156, 158 passim; quiz 162.
5. B. R. Chrcanovic and M. H. Abreu, *Oral and maxillofacial surgery*, 2013, **17**, 81-93.
6. K. G. Neoh, X. Hu, D. Zheng and E. T. Kang, *Biomaterials*, 2012, **33**, 2813-2822.
7. L. Zhao, P. K. Chu, Y. Zhang and Z. Wu, *Journal of biomedical materials research. Part B, Applied biomaterials*, 2009, **91**, 470-480.
8. T. Albrektsson, P. I. Branemark, H. A. Hansson and J. Lindstrom, *Acta orthopaedica Scandinavica*, 1981, **52**, 155-170.
9. K. Kulangara and K. W. Leong, *Soft Matter*, 2009, **5**, 4072-4076.
10. T. Albrektsson and A. Wennerberg, *The International journal of prosthodontics*, 2004, **17**, 536-543.
11. G. Zhao, A. L. Raines, M. Wieland, Z. Schwartz and B. D. Boyan, *Biomaterials*, 2007, **28**, 2821-2829.
12. K. Takeuchi, L. Saruwatari, H. K. Nakamura, J. M. Yang and T. Ogawa, *Journal of biomedical materials research. Part A*, 2005, **72**, 296-305.
13. L. C. Hsu, J. Fang, D. A. Borca-Tasciuc, R. W. Worobo and C. I. Moraru, *Applied and environmental microbiology*, 2013, **79**, 2703-2712.
14. L. Rizzello, R. Cingolani and P. P. Pompa, *Nanomedicine*, 2013, **8**, 807-821.
15. A. G. Gristina, *Science*, 1987, **237**, 1588-1595.
16. B. M. Geilich and T. J. Webster, *International journal of nanomedicine*, 2013, **8**, 1177-1184.
17. H. K. Webb, V. Boshkovikj, C. J. Fluke, V. K. Truong, J. Hasan, V. A. Baulin, R. Lapovok, Y. Estrin, R. J. Crawford and E. P. Ivanova, *Biofouling*, 2013, **29**, 163-170.
18. L. Zhao, H. Wang, K. Huo, L. Cui, W. Zhang, H. Ni, Y. Zhang, Z. Wu and P. K. Chu, *Biomaterials*, 2011, **32**, 5706-5716.
19. J. Hasan, R. J. Crawford and E. P. Ivanova, *Trends in biotechnology*, 2013, **31**, 295-304.
20. G. A. Fielding, M. Roy, A. Bandyopadhyay and S. Bose, *Acta biomaterialia*, 2012, **8**, 3144-3152.
21. K. Huo, X. Zhang, H. Wang, L. Zhao, X. Liu and P. K. Chu, *Biomaterials*, 2013, **34**, 3467-3478.
22. W. Att, N. Hori, M. Takeuchi, J. Ouyang, Y. Yang, M. Anpo and T. Ogawa, *Biomaterials*, 2009, **30**, 5352-5363.
23. N. Hori, W. Att, T. Ueno, N. Sato, M. Yamada, L. Saruwatari, T. Suzuki and T. Ogawa, *Journal of dental research*, 2009, **88**, 663-667.
24. F. Iwasa, N. Hori, T. Ueno, H. Minamikawa, M. Yamada and T. Ogawa, *Biomaterials*, 2010, **31**, 2717-2727.
25. W. F. Stickle and J. F. Moulder, *Journal of Vacuum Science & Technology A*, 1991, **9**, 1441-1446.
26. M. Quirynen and C. M. Bollen, *Journal of clinical periodontology*, 1995, **22**, 1-14.
27. J. Vlacic-Zischke, S. M. Hamlet, T. Friis, M. S. Tonetti and S. Ivanovski, *Biomaterials*, 2011, **32**, 665-671.
28. G. Zhao, Z. Schwartz, M. Wieland, F. Rupp, J. Geis-Gerstorfer, D. L. Cochran and B. D. Boyan, *Journal of biomedical materials research. Part A*, 2005, **74**, 49-58.
29. C. Sittig, M. Textor, N. D. Spencer, M. Wieland and P. H. Vallotton, *Journal of materials science. Materials in medicine*, 1999, **10**, 35-46.
30. F. Variola, J. H. Yi, L. Richert, J. D. Wuest, F. Rosei and A. Nanci, *Biomaterials*, 2008, **29**, 1285-1298.
31. L. Feng, S. Li, Y. Li, H. Li, L. Zhang, J. Zhai, Y. Song, B. Liu, L. Jiang and D. Zhu, *Advanced Materials*, 2002, **14**, 1857-1860.
32. X. Gao and L. Jiang, *Nature*, 2004, **432**, 36-36.
33. J. Bico, C. Tordeux and D. Quéré, *EPL (Europhysics Letters)*, 2001, **55**, 214.
34. L. Hall-Stoodley, J. W. Costerton and P. Stoodley, *Nature reviews. Microbiology*, 2004, **2**, 95-108.
35. E. M. Hetrick and M. H. Schoenfisch, *Chemical Society reviews*, 2006, **35**, 780-789.
36. L. Ploux, A. Ponche and K. Anselme, *Journal of Adhesion Science and Technology*, 2010, **24**, 2165-2201.
37. A. Pierres, A. M. Benoliel, D. Touchard and P. Bongrand, *Biophysical journal*, 2008, **94**, 4114-4122.
38. K. Anselme, P. Davidson, A. M. Popa, M. Giazzon, M. Liley and L. Ploux, *Acta biomaterialia*, 2010, **6**, 3824-3846.
39. M. Katsikogianni and Y. F. Missirlis, *European cells & materials*, 2004, **8**, 37-57.
40. A. Okada, T. Nikaido, M. Ikeda, K. Okada, J. Yamauchi, R. M. Foxton, H. Sawada, J. Tagami and K. Matin, *Dental Materials Journal*, 2008, **27**, 565-572.
41. J. Tsibouklis, M. Stone, A. A. Thorpe, P. Graham, V. Peters, R. Heerlien, J. R. Smith, K. L. Green and T. G. Nevell, *Biomaterials*, 1999, **20**, 1229-1235.
42. Y.-Y. Luk, M. Kato and M. Mrksich, *Langmuir : the ACS journal of surfaces and colloids*, 2000, **16**, 9604-9608.
43. P. Tang, W. Zhang, Y. Wang, B. Zhang, H. Wang, C. Lin and L. Zhang, *Journal of Nanomaterials*, 2011, **2011**.

44. N. P. Lang, G. E. Salvi, G. Huynh-Ba, S. Ivanovski, N. Donos and D. D. Bosshardt, *Clinical oral implants research*, 2011, **22**, 349-356.
45. J. L. Dalsin and P. B. Messersmith, *Materials Today*, 2005, **8**, 38-46.
46. M. C. Siebers, P. J. ter Brugge, X. F. Walboomers and J. A. Jansen, *Biomaterials*, 2005, **26**, 137-146.
47. E. A. Cavalcanti-Adam, A. Micoulet, J. Blummel, J. Auernheimer, H. Kessler and J. P. Spatz, *European journal of cell biology*, 2006, **85**, 219-224.
48. M. Textor, C. Sittig, V. Frauchiger, S. Tosatti and D. M. Brunette, in *Titanium in medicine*, eds. D. M. Brunette, P. Tengvall, M. Textor and P. Thomsen, Springer, Berlin, 2001, pp. 171-230.
49. S. Mori and D. B. Burr, *Bone*, 1993, **14**, 103-109.
50. A. Boyde, N. N. Ali and S. J. Jones, *Scanning electron microscopy*, 1985, 1259-1271.
51. B. D. Boyan, S. Lossdorfer, L. Wang, G. Zhao, C. H. Lohmann, D. L. Cochran and Z. Schwartz, *European cells & materials*, 2003, **6**, 22-27.
52. W. Att, N. Hori, F. Iwasa, M. Yamada, T. Ueno and T. Ogawa, *Biomaterials*, 2009, **30**, 4268-4276.
53. D. McQeen, J. E. Sundgreen, B. Ivarsson, I. Lundstrom, B. Ekstam, A. Stevensson and P. I. Brånemark, in *Advances in biomaterials*, eds. A. J. C. Lee, T. Albrektsson and P. I. Brånemark, Technomic publishing company, Western hemisphere, 1982, pp. 179-185.
54. T. Albrektsson and M. Jacobsson, *The Journal of prosthetic dentistry*, 1987, **57**, 597-607.
55. R. Wang, K. Hashimoto, A. Fujishima, M. Chikuni, E. Kojima, A. Kitamura, M. Shimohigoshi and T. Watanabe, *Nature*, 1997, **388**, 431-432.
56. T. Matsunaga, R. Tomoda, T. Nakajima and H. Wake, *FEMS Microbiology Letters*, 1985, **29**, 211-214.
57. M. A. Henderson, *Surface Science*, 1996, **355**, 151-166.
58. T. Sawase, R. Jimbo, K. Baba, Y. Shibata, T. Ikeda and M. Atsuta, *Clinical oral implants research*, 2008, **19**, 491-496.
59. M. B. Hugenschmidt, L. Gamble and C. T. Campbell, *Surface Science*, 1994, **302**, 329-340.
60. D. Buser, N. Broggini, M. Wieland, R. K. Schenk, A. J. Denzer, D. L. Cochran, B. Hoffmann, A. Lussi and S. G. Steinemann, *Journal of dental research*, 2004, **83**, 529-533.
61. D. K. Owens and R. C. Wendt, *Journal of Applied Polymer Science*, 1969, **13**, 1741-1747.
62. Q. Luo, Y. Huang, X. Deng, J. Zhang, X. Li, S. Zhao and X. Li, *Nanomedicine*, 2013, **8**, 739-755.
63. Y. Huang, G. Zha, Q. Luo, J. Zhang, F. Zhang, X. Li, S. Zhao, W. Zhu and X. Li, *Scientific reports*, 2014, **4**, 6172.
64. M. D. Koutsoudis, D. Tsaltas, T. D. Minogue and S. B. von Bodman, *Proceedings of the National Academy of Sciences of the United States of America*, 2006, **103**, 5983-5988.

Table of content

Topography-dependent antibacterial, osteogenic properties of pure titanium and its biological aging mechanism.